

# Reference Point Specification in Hypervolume Calculation for Fair Comparison and Efficient Search

Hisao Ishibuchi<sup>1)2)</sup>

<sup>1)</sup>Southern University of Science and Technology (SUSTech)  
Shenzhen, Guangdong, China

Ryo Imada<sup>2)</sup>, Yu Setoguchi<sup>2)</sup>, Yusuke Nojima<sup>2)</sup>

<sup>2)</sup>Osaka Prefecture University  
Sakai, Osaka, Japan  
{hisaoi@, yu.setoguchi@ci., ryo.imada@ci., nojima@}cs.osakafu-u.ac.jp

## ABSTRACT

Hypervolume has been frequently used as a performance indicator for comparing evolutionary multiobjective optimization (EMO) algorithms. Hypervolume has been also used in indicator-based algorithms. Whereas a reference point is needed for hypervolume calculation, its specification has not been discussed in detail from a viewpoint of fair comparison. This may be because a slightly worse reference point than the nadir point seems to work well. In this paper, we tackle this issue: How to specify a reference point for fair comparison. First we discuss an appropriate specification of a reference point for multiobjective problems. Our discussions are based on the well-known theoretical results about the optimal solution distribution for hypervolume maximization. Next we examine various specifications by computational experiments. Experimental results show that a slightly worse reference point than the nadir point works well only for test problems with triangular Pareto fronts. Then we explain why this specification is not always appropriate for test problems with inverted triangular Pareto fronts. We also report a number of solution sets obtained by SMS-EMOA with various specifications of a reference point.

## CCS CONCEPTS

• **Mathematics of computing** → **Optimization algorithms**

## KEYWORDS

Evolutionary multiobjective optimization, hypervolume

## ACM Reference format:

H. Ishibuchi, R. Imada, Y. Setoguchi, and Y. Nojima. 2017. Reference Point Specification in Hypervolume Calculation for Fair Comparison and Efficient Search. In *Proceedings of the Genetic and Evolutionary Computation Conference 2017, Berlin, Germany, July 15–19, 2017 (GECCO '17)*, 8 pages. DOI: 10.1145/3071178.3071264

Permission to make digital or hard copies of all or part of this work for personal or classroom use is granted without fee provided that copies are not made or distributed for profit or commercial advantage and that copies bear this notice and the full citation on the first page. Copyrights for components of this work owned by others than the author(s) must be honored. Abstracting with credit is permitted. To copy otherwise, or republish, to post on servers or to redistribute to lists, requires prior specific permission and/or a fee. Request permissions from [Permissions@acm.org](mailto:Permissions@acm.org).  
GECCO '17, July 15-19, 2017, Berlin, Germany  
Copyright is held by the owner/author(s). Publication rights licensed to ACM.  
ACM 978-1-4503-4920-8/17/07...\$15.00  
DOI: <http://dx.doi.org/10.1145/3071178.3071264>

## 1 INTRODUCTION

In the field of evolutionary multiobjective optimization (EMO), new algorithms continue to be proposed every year. The proposed algorithms are compared with existing ones using performance indicators. The hypervolume [26] has been the most frequently-used indicator while a wide variety of choices have been proposed in the literature [27]. This may be because no other Pareto compliant indicator is known [25]. The hypervolume has also been used in indicator-based EMO algorithms such as SMS-EMOA [4] and HypE [2]. In these algorithms, multiobjective optimization is handled as a single-objective problem to search for a solution set with the maximum hypervolume.

One related research question is the optimal distribution of solutions for hypervolume maximization. Theoretical studies [1, 6, 8] show that the hypervolume is maximized by a set of uniformly distributed solutions with the same distance between adjacent solutions when the Pareto front of a two-objective problem is a straight line. It is also shown that such a solution set is not the optimal when the Pareto front is nonlinear. Except for the case of single-dimensional degenerate Pareto fronts [20], no optimal distribution of solutions has been theoretically derived for multiobjective problems with three or more objectives (see [13]).

Selection of a pre-specified number of solutions from a given solution set has been studied for hypervolume maximization under the name of hypervolume subset selection [3, 5, 9, 10, 17]. This is a single-objective combinatorial optimization problem. This can be also viewed as a pre-processing procedure for selecting a small number of solutions from a large number of obtained solutions by EMO algorithms [14]. Efficient subset selection methods have been proposed in the literature [3, 5, 9, 10, 16].

A reference point is needed for hypervolume calculation. For two-objective problems, its effect on the optimal distribution of solutions for hypervolume maximization has been theoretically studied [1, 6, 8]. It is also shown that performance comparison results among different EMO algorithms depend on the location of a reference point [12, 13, 14, 15]. However, to the best of our knowledge, reference point specification has not been studied in detail from a viewpoint of fair performance comparison, especially for many-objective problems. A different specification was used in a different study. For example, the reference point was specified for a many-objective DTLZ1 problem [7] with the nadir point (0.5, ..., 0.5) as follows: (0.505, ..., 0.505) in Seada & Deb [19], (0.55, ..., 0.55) in Yuan et al. [22, 23], (0.7, ..., 0.7) in Wagner et al. [21], and (1.0, ..., 1.0) in Li et al. [18].

In this paper, we discuss reference point specification for fair comparison of different EMO algorithms for multiobjective and many-objective problems. Our idea is based on the following two assumptions with respect to performance evaluation of solution sets by the hypervolume:

(i) A uniformly distributed solution set over the entire linear Pareto front should be highly evaluated by the hypervolume. This means that such a solution set should have a large hypervolume value.

(ii) Any solution in a solution set should not have a dominant effect on the hypervolume. This means that all solutions should have similar hypervolume contributions.

This paper is organized as follows. In Section 2, we discuss these two assumptions based on the optimal solution distribution for hypervolume maximization for a linear Pareto front of a two-objective problem. If the reference point is not too close to the Pareto front, its location has no effect on the optimal solution distribution. However, the relative importance of the two extreme solutions increases as the distance between the reference point and the Pareto front increases. Based on the theoretical studies [1, 6, 8], we explain that an appropriate specification of the reference point depends on the size of solution sets to be evaluated (i.e., the number of solutions). In Section 3, we discuss the reference point specification for multiobjective problems with three or more objectives. We show that an appropriate specification of the reference point depends on the size of solution sets, the number of objectives and the shape of the Pareto front. In Section 4, we report our experimental results where different solution sets are compared using the hypervolume with a different reference point. In Section 5, we examine the effect of the reference point on the search ability of SMS-EMOA [4] by computational experiments. Finally we conclude this paper in Section 6.

## 2 REFERENCE POINT SPECIFICATION FOR TWO-OBJECTIVE PROBLEMS

Let us consider a two-objective minimization problem with a linear Pareto front, which is the straight line between  $(0, 1)$  and  $(1, 0)$  in the objective space. This Pareto front can be represented by the following equations:  $f_1 + f_2 = 1$  and  $0 \leq f_i \leq 1$  for  $i = 1, 2$  where  $f_1$  and  $f_2$  are the first and the second objective, respectively.

In Fig. 1, we show uniformly distributed solution sets with the same distance between adjacent solutions. The number of solutions in each solution set in Fig. 1 is 3 in (a), 5 in (b) and 10 in (c). Let us assume that the reference point is given by  $(r, r)$ . As shown in [1, 6, 8], these solution sets are optimal distributions of solutions for hypervolume maximization when  $r \geq 1.5$  in Fig. 1 (a),  $r \geq 1.25$  in Fig. 1 (b), and  $r \geq 1.1$  in Fig. 1 (c). In Fig. 2, we show the optimal distributions of five solutions for  $r = 1.1, 1.25$  and  $1.5$  (see [1, 6, 8]). As shown in Fig. 2 (a), the two extreme solutions (i.e., the edges of the Pareto front) are not included in the optimal solution set for hypervolume maximization when  $r < 1.25$ . When the Pareto front is the straight line between  $(0, 1)$  and  $(1, 0)$  as in Fig. 1 and Fig. 2, the two extreme solutions are included in the optimal solution set if and only if  $r \geq 1 + 1/(n-1)$  where  $n$  is the number of solutions (for more general discussions, see [1, 6, 8]).

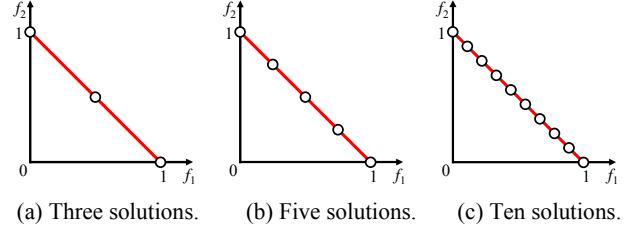


Figure 1: Uniformly distributed solutions.

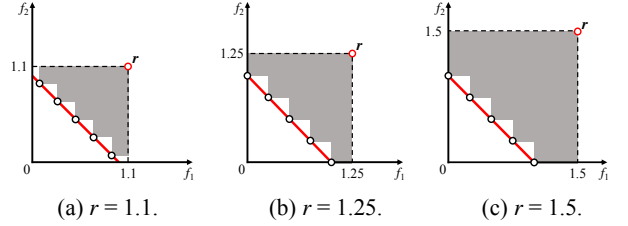


Figure 2: Optimal distributions of five solutions.

From the above discussions, one may think that any reference point  $(r, r)$  can be used as far as  $r \geq 1 + 1/(n-1)$  since the uniformly distributed solution set including the two extreme solutions is optimal for hypervolume maximization. However, hypervolume contributions of the two extreme solutions (and thus the relative importance of each solution) depend on the location of the reference point as shown in Fig. 3.

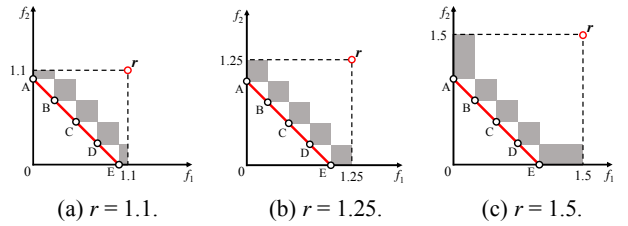


Figure 3: Hypervolume contribution of each solution.

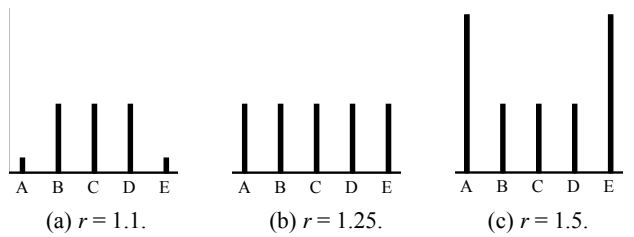


Figure 4: Comparison of hypervolume contribution in Fig. 3.

The hypervolume contribution of each solution is also shown in Fig. 4. The hypervolume contributions of all solutions are the same when  $r = 1.25$  in Fig. 3 (b). In this case, all the following five solution sets have the same hypervolume value in Fig. 3 (b):  $\{A, B, C, D\}$ ,  $\{A, B, C, E\}$ ,  $\{A, B, D, E\}$ ,  $\{A, C, D, E\}$ ,  $\{B, C, D, E\}$  where a single solution is removed from the original solution set. However, in Fig. 3 (c), the three solution sets  $\{A, B, C, E\}$ ,  $\{A, B, D, E\}$  and  $\{A, C, D, E\}$  with the two extreme solutions A and E have larger hypervolume values than the other two solution

sets. This is because the two extreme solutions have larger hypervolume contributions than the others in Fig. 3 (c).

If we have a clear reason for believing that the two extreme solutions are more important than the others, it is a good idea to specify the reference point  $(r, r)$  so that  $r > 1+1/(n-1)$  holds. Except for this case, our suggestion is to specify the reference point  $(r, r)$  as  $r = 1+1/(n-1)$ . In general, the Pareto front is not the straight line between  $(0, 1)$  and  $(1, 0)$  in the objective space. However, we can normalize the objective space of a two-objective problem so that the ideal and the nadir point are  $(0, 0)$  and  $(1, 1)$ , respectively. After this normalization, the reference point  $(r, r)$  with  $r = 1+1/(n-1)$  may be a good choice even when the Pareto front is nonlinear. This suggestion is exactly the same as the 1% worse point than the nadir point when the population size is 101. This specification was used in Seada & Deb [19].

### 3 REFERENCE POINT SPECIFICATION FOR THREE OR MORE OBJECTIVES

#### 3.1 For Triangular Pareto Fronts

Let us consider an  $m$ -objective minimization problem with a linear triangular Pareto front, which is specified by  $f_1 + f_2 + \dots + f_m = 1$  and  $0 \leq f_i \leq 1$  for  $i = 1, 2, \dots, m$ . This is the same as the Pareto front of DTLZ1 [7] after the normalization. DTLZ2-4 [7] and WFG4-9 [11] have similar Pareto fronts:  $f_1^2 + f_2^2 + \dots + f_m^2 = 1$  and  $0 \leq f_i \leq 1$  for  $i = 1, 2, \dots, m$  after the normalization.

In Figs. 5-7, we show the linear Pareto front for the case of three objectives together with uniformly distributed solutions, which are specified in the same manner as the weight vector specification in MOEA/D [24]. In each plot in these figures, the relative size of the hypervolume contribution of each solution is shown by the radius of the corresponding circle. In Fig. 5, the three extreme solutions have no hypervolume contribution. So, they are not shown in Fig. 5. The hypervolume contributions of all solutions are the same in Fig. 6 (d) and Fig. 7 (a).

When  $r = 1.0$  (i.e., the nadir point), all solutions except for the three extreme solutions have the same hypervolume contributions in Fig. 5. Thus the use of the nadir point is not so bad in Fig. 5. However,  $r = 1.1$  may be a better specification since all solutions have the same hypervolume contributions in Fig. 6 (d). In Fig. 7 with  $r = 1.5$ , the three extreme solutions have much larger hypervolume contributions than the other solutions in Fig. 7 (b)-(d). Thus  $r = 1.5$  is not a good specification. However,  $r = 1.5$  seems to be a good specification in Fig. 7 (a) with 6 solutions.

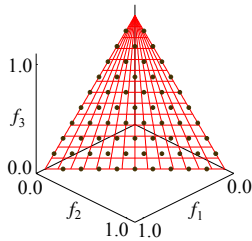


Figure 5: Hypervolume contribution: 66 solutions ( $r = 1.0$ ).

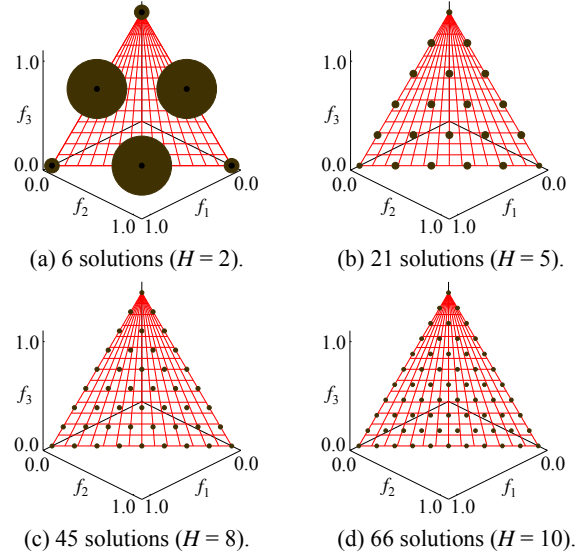


Figure 6: Hypervolume contribution ( $r = 1.1$ ).

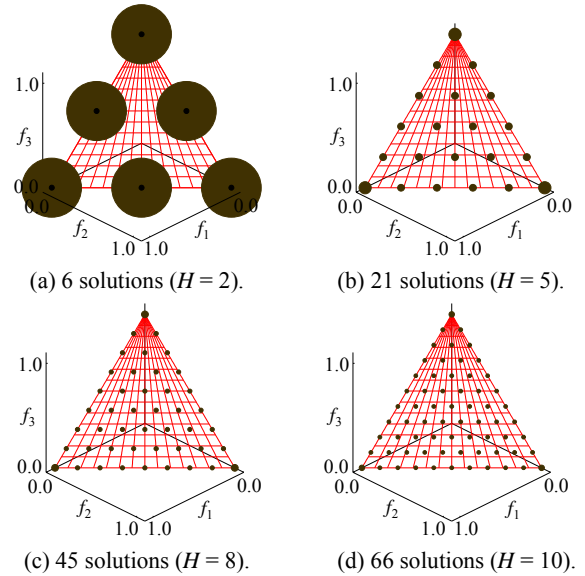


Figure 7: Hypervolume contribution ( $r = 1.5$ ).

For two-objective problems in Section 2, we suggested the following specification of the reference point  $(r, r)$ :  $r = 1+1/(n-1)$  where  $n$  is the number of solutions. Let us denote the number of solutions on each line between the two extreme solutions in Figs. 5-7 by  $K$  including the two extreme solutions (e.g.,  $K = 3$  in Fig. 7 (a),  $K = 6$  in Fig. 7 (b)). Using the user-defined parameter  $H$  for specifying the number of weight vectors in MOEA/D,  $K$  is written as  $K = H + 1$ . When all solutions are uniformly distributed over the entire Pareto front, the distance between adjacent solutions is  $2^{1/2}/(n-1)$  in Section 2 and  $2^{1/2}/(K-1)$  in this section. That is,  $n$  and  $K$  can be viewed as playing the same role in the uniformly distributed solution sets. Thus we extend our suggestion in Section 2 to  $r = 1+1/(K-1) = 1+1/H$ . The suggested reference

point for each plot in Figs. 6-7 is as follows:  $r = 1.5$  for (a) with 6 solutions,  $r = 1.2$  for (b) with 21 solutions,  $r = 1.125$  for (c) with 45 solutions, and  $r = 1.1$  for (d) with 66 solutions. This suggestion is the same as the value of  $r$  in Fig. 6 (a) and Fig. 7 (d) where all solutions have the same hypervolume contribution.

In MOEA/D [24], the population size  $n_{pop}$  is calculated for an  $m$ -objective problem using the user-defined parameter  $H$  as

$$n_{pop} = C_{H+m-1}^{m-1} \quad (1)$$

Let  $n$  be the number of solutions in each solution set to be compared. In general,  $n$  cannot be written in the form of (1). Thus we first specify the value of  $H$  using the following relation:

$$C_{H+m-1}^{m-1} \leq n < C_{H+m}^{m-1} \quad (2)$$

Then we calculate the value of  $r$  as  $r = 1 + 1/H$ . This is our suggested reference point specification for  $m$ -objective problems.

### 3.2 For Inverted Triangular Pareto Fronts

The Pareto front of the inverted  $m$ -objective DTLZ1 [16] can be written in the normalized objective space as follows:  $f_1 + f_2 + \dots + f_m = m - 1$  and  $0 \leq f_i \leq 1$  for  $i = 1, 2, \dots, m$ . This Pareto front is shown in Fig. 8 for the case of three objectives (i.e.,  $m = 3$ ).

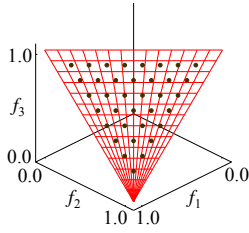


**Figure 8:** Hypervolume contribution: 66 solutions ( $r = 1.0$ ).

In the same manner as in Figs. 5-7, we show the relative size of the hypervolume contribution of each solution in Figs. 8-10. In Fig. 8, all solutions on the sides (i.e., boundary) of the inverted triangular Pareto front have no hypervolume contribution. Thus they are not shown in Fig. 8. In Fig. 9 (d) and Fig. 10 (a), all solutions have the same hypervolume contribution. This supports our suggested reference point specification:  $r = 1.1$  for  $H = 10$  and  $r = 1.5$  for  $H = 2$ . The inside solutions in Fig. 9 (b) have larger hypervolume contributions whereas the boundary solutions in Fig. 10 (b) have larger contributions.

In Fig. 10 (b)-(c), solutions on the sides of the inverted triangular Pareto front have larger hypervolume contributions than the inside solutions. However, in Fig. 7 (b)-(c), all solutions except for the three extreme solutions have the same hypervolume contribution. This difference can be explained by projecting the two types of Pareto fronts to a two-dimensional subspace as in Fig. 11. In Fig. 11 (a), only the extreme solution at  $(0, 0)$  is non-dominated. Thus, only this solution has a positive hypervolume contribution in the  $f_2$ - $f_3$  space. By moving the reference point away from the Pareto front along the  $f_1$  axis, the hypervolume contribution of only this extreme solution increases in the original three-dimensional objective space. This is the reason why the

increase in the value of  $r$  (i.e., the move of the reference point away from the Pareto front) increases the hypervolume contributions of only the three extreme solutions in Figs. 5-7.

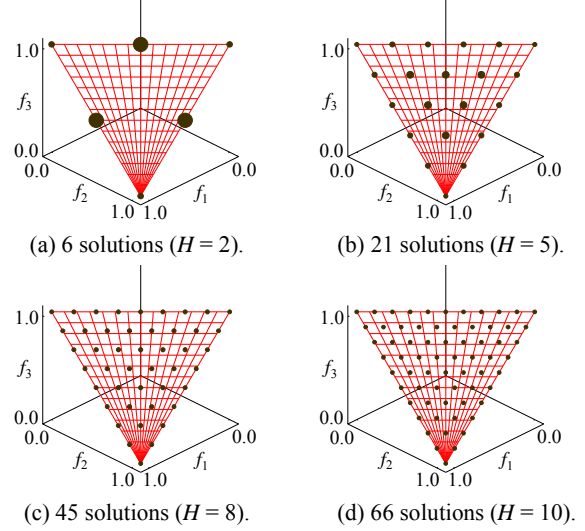


**Figure 9:** Hypervolume contribution ( $r = 1.1$ ).

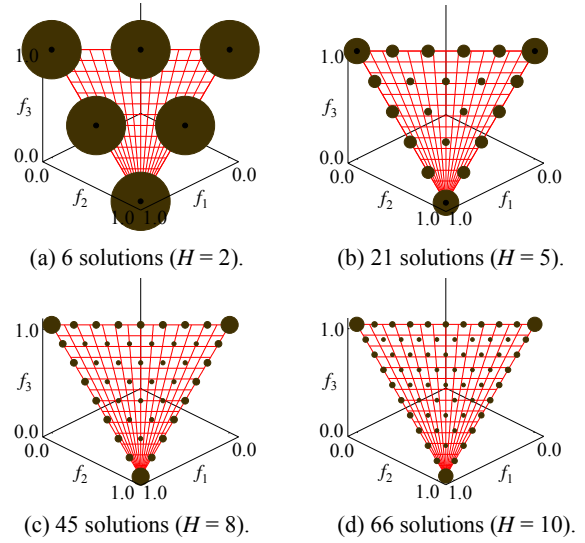


**Figure 10:** Hypervolume contribution ( $r = 1.5$ ).

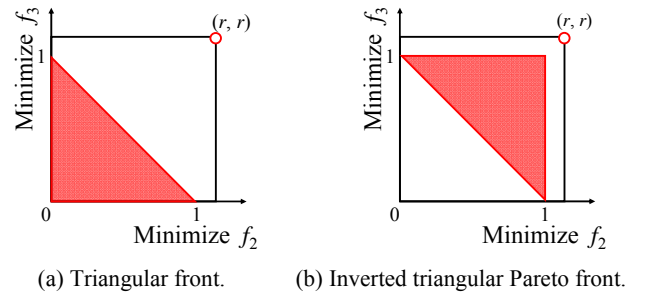


**Figure 11:** Projection of the Pareto front to the  $f_2$ - $f_3$  space.

However, in Fig. 11 (b), all solutions on the line between (1, 0) and (0, 1) are non-dominated in the  $f_2$ - $f_3$  space. This means that all solutions on this line have positive hypervolume contributions. As a result, by moving the reference point away from the Pareto front along the  $f_1$  axis, the hypervolume contributions of all solutions along this line monotonically increase in the original three-dimensional objective space. This is the reason why the increase in the value of  $r$  (i.e., the move of the reference point away from the Pareto front) increases the hypervolume contributions of all solutions along the sides of the inverted triangular Pareto front in Figs. 8-10. When the reference point is far away from the Pareto front (e.g.,  $r = 20$ ), the hypervolume contributions of boundary solutions are much larger than those of inside solutions. As a result, no inside solutions are included in the optimal solution set (for details, see our former study [13]).

From the comparison between Figs. 5-7 and Figs. 8-10, we can see that the hypervolume contribution of each solution strongly depends on the shape of the Pareto front. Whereas  $r = 1.0$  in Fig. 5 and  $r = 1.1$  in Fig. 7 (b) seem to be good specifications, they clearly look inappropriate in Fig. 8 and Fig. 10 (b).

The reason for the difference between Fig. 5 and Fig. 8 is that the hypervolume is calculated from the top-right corner using the inverted triangular front surface as shown in Fig. 12 (a). Thus the region of the Pareto front where the hypervolume is calculated perfectly overlaps with the inverted triangular Pareto front as shown in Fig. 12 (b) when  $r = 1.0$ . This means that all solutions on the boundary of the inverted triangular Pareto front have no hypervolume contribution when the reference point is the nadir point (i.e.,  $r = 1.0$ ). However, as shown in Fig. 12 (c) and Fig. 12 (d), only the three extreme solutions of the triangular Pareto front are on the boundary of the hypervolume calculation region. Thus all solutions except for the three extreme solutions have positive hypervolume contributions even when the reference point is the nadir point (see Fig. 5).

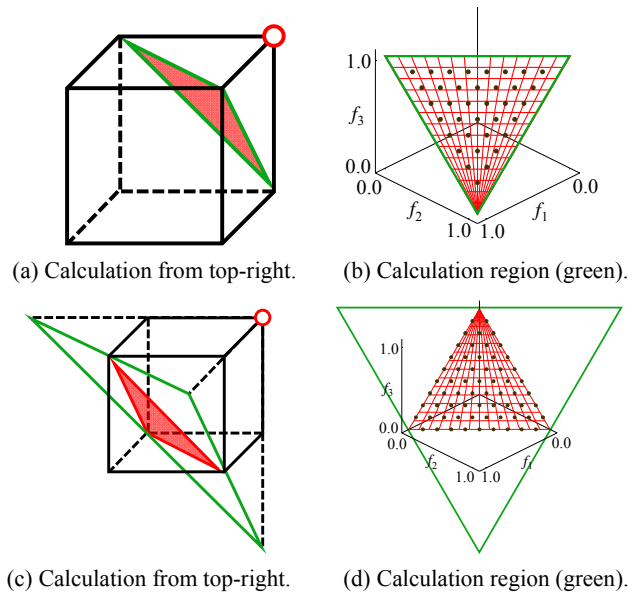


Figure 12: Illustration of the hypervolume calculation.

## 4 COMPARISON OF DIFFERENT SOLUTION SETS BY THE HYPERVOLUME

### 4.1 Triangular Pareto Front

In this section, we compare a number of artificially generated solution sets using the hypervolume. First we generate a set of uniformly distributed 91 solutions by specifying the value of  $H$  as  $H = 12$  in the weight vector specification mechanism in MOEA/D [24] as shown in the upper-right plot in Fig. 13. Let us denote the distance between two adjacent solutions by  $l$  as shown in the upper-right plot in Fig. 13. Then we shrink the size of the solution distribution by changing the distance between solutions from  $l$  to  $0.5l, 0.55l, \dots, 0.95l$  as explained in the upper part of Fig. 13. We also increase the distance from  $l$  to  $1.05l, 1.1l, \dots, 1.5l$  as shown in the lower part of Fig. 13. All solutions outside the Pareto front are uniformly relocated along the sides of the Pareto front.

Since  $H = 12$ , our suggestion for the reference point specification is  $r = 1 + 1/H = 13/12 \cong 1.0833$ . Using three reference point specifications ( $r = 1.01, 13/12, 1.5$ ), we compared the generated 21 solution sets by the hypervolume. In Fig. 14, we show the hypervolume-based comparison results of the 21 solution sets. The calculated hypervolume values are normalized in Fig. 14 so that the largest hypervolume value becomes 1.0 for each specification of the reference point. In Fig. 14, the solution set with the distance  $1.0l$  (i.e., the original solution set generated by the weight vector specification method) is evaluated as the best solution set in all the three reference point specifications.

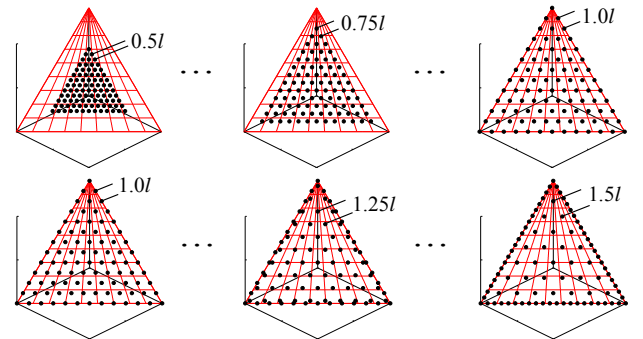


Figure 13: Explanations of the generated solution sets.

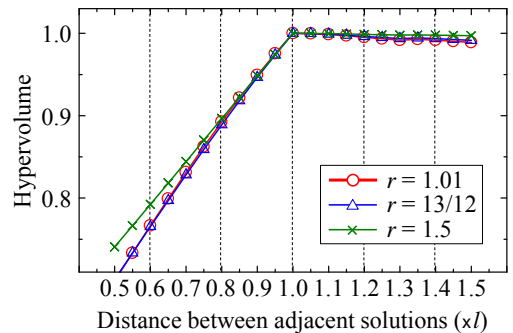
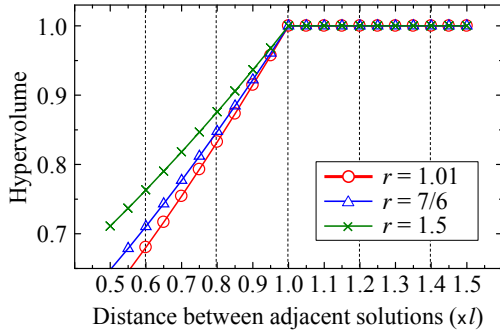


Figure 14: Comparison results for the triangular three-objective Pareto front ( $H = 12, r = 1.01, 13/12, 1.5$ ).



**Figure 15:** Comparison results for the triangular five-objective Pareto front ( $H = 6$ ,  $r = 1.01, 7/6, 1.5$ ).

In the same manner as Fig. 13, we generate 21 solution sets on the triangular-shape Pareto front of a five-objective problem. First, a set of uniformly distributed 210 solutions is generated by specifying the value of  $H$  as  $H = 6$ . Then the other 20 solution sets are generated by changing the distance between adjacent solutions from  $l$  to  $0.5l, 0.55l, 0.6l, \dots, 1.5l$ . Among the generated 210 solutions by specifying  $H$  as  $H = 6$  for a five-objective problem, 205 solutions are boundary solutions (i.e., only five solutions are inside the Pareto front). When we increase the distance between the adjacent solutions, we change the locations of only the five inside solutions since all the other 205 solutions are on the boundary of the Pareto front. When we decrease the distance, we change the locations of all the 210 solutions. By decreasing the distance between adjacent solutions, all the 210 solutions become inside solutions (see Fig. 13).

Since  $H = 6$ , our suggestion for the reference point specification is  $r = 1 + 1/H = 7/6 \approx 1.1667$ . Using three reference point specifications ( $r = 1.01, 7/6, 1.5$ ), we compare the generated 21 solution sets. As in Fig. 14, we obtain the similar results from the three specifications of the reference point in Fig. 15.

## 4.2 Inverted Triangular Pareto Front

The generated solution sets in the previous subsection are inverted as shown in 16 in this subsection. In the same manner as in Fig. 14, the inverted solution sets are compared by the hypervolume using the three reference point specifications:  $r = 1.01, 13/12, 1.5$ . Experimental results are shown in Fig. 17.

Fig. 17 shows that the performance comparison results strongly depend on the reference point specification. When the reference point is close to the nadir point (i.e., when  $r = 1.01$ ), the best evaluation is obtained for the solution set with the solution distance  $0.8l$ . That is, a shrunk solution set is evaluated as being the best for  $r = 1.01$ . When the reference point is far from the nadir point (i.e.,  $r = 1.5$ ), the best evaluation is obtained for the solution set with the solution distance  $1.35l$ . That is, a solution set with a large number of solutions around the sides of the inverted triangular Pareto front is evaluated as being the best for  $r = 1.5$ . When the suggested value (i.e.,  $r = 13/12$ ) is used, the original solution set with the solution distance  $1.0l$  and some similar solution sets have high hypervolume values in Fig. 17. That is, intuitively acceptable results are obtained from  $r = 13/12$ .

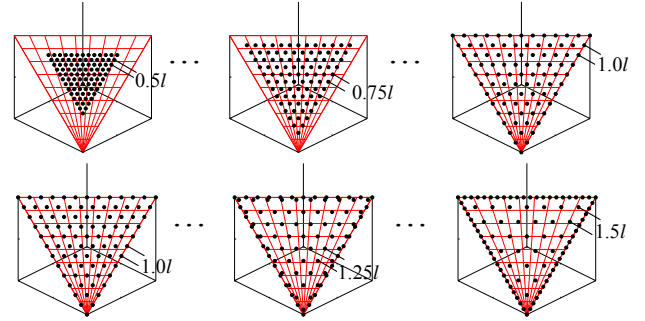


**Figure 16:** Explanations of the inverted solution sets.

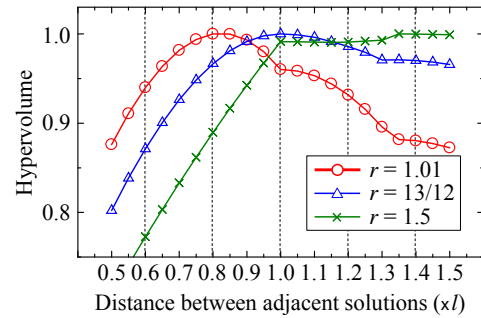


**Figure 17:** Comparison results for the inverted triangular three-objective Pareto front ( $H = 12$ ,  $r = 1.01, 13/12, 1.5$ ).

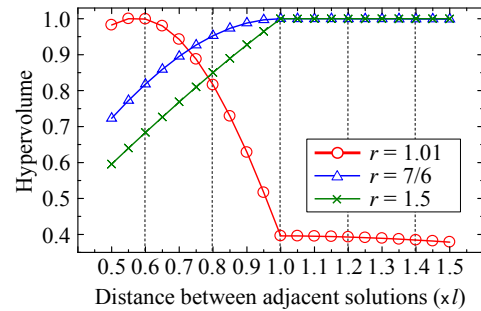


**Figure 18:** Comparison results for the inverted triangular five-objective Pareto front ( $H = 6$ ,  $r = 1.01, 7/6, 1.5$ ).

We also evaluate the inverted solution sets of a five-objective problem using the three reference point specifications:  $r = 1.01, 7/6, 1.5$ . Experimental results are shown in Fig. 18. When  $r = 1.01$ , a shrunk solution set with the solution distance  $0.55l$  is evaluated as the best solution set by the hypervolume. When the suggested specification (i.e.,  $r = 7/6$ ) and  $r = 1.5$  are used, the original solution set with the solution distance  $l$  and some similar solution sets have large hypervolume values in Fig. 18. It should be noted that the locations of only the five inside solutions are changed when the distance between adjacent solutions is increased.

## 5 EFFECT ON THE SEARCH OF SMS-EMOA

In this section, we report experimental results of SMS-EMOA [4] on the three-objective DTLZ1 and inverted DTLZ1 problems.

Some results are also shown for the five-objective inverted DTLZ1 problem. We performed computational experiments under the following setting:

- Number of distance variables: 5,
- Population size ( $n_{pop}$ ): 15 and 100,
- Crossover: SBX with the index 20 (probability: 1.0),
- Mutation: Polynomial mutation with the index 20 (probability:  $1/L$  where  $L$  is the string length),
- Termination conditions: 100,000 generations,
- Number of runs: 5.

Three reference point specifications ( $r = 1.0, 1.1, 1.5$ ) are examined in the normalized objective space. The normalization is performed using non-dominated solutions among solutions in the current population at each generation. It should be noted that our suggested reference point is as follows:  $r = 1.25$  ( $m = 3, n_{pop} = 15, H = 4$ ),  $r = 1.08333$  ( $m = 3, n_{pop} = 100, H = 12$ ),  $r = 1.5$  ( $m = 5, n_{pop} = 15, H = 2$ ),  $r = 1.25$  ( $m = 5, n_{pop} = 100, H = 4$ ).

Obtained solution sets are shown for the three-objective DTLZ1 and inverted DTLZ1 problems in Figs. 19-24. When  $r = 1.0$  (i.e., nadir point) in Fig. 19 and Fig. 22, good solution sets are not obtained. This is because the extreme solutions in the current population are likely to be removed since they have no hypervolume contribution. When  $r = 1.1$  in Fig. 20 and Fig. 23, good solution sets are obtained only when the population size is 100. This is consistent with our suggested specification (i.e.,  $r = 1.08333$  for the case of the population size 100). When  $r = 1.5$ , many solutions are obtained on the sides of the inverted triangular Pareto front in Fig. 24 whereas uniformly distributed solutions are obtained in Fig. 21 for the triangular Pareto front. These results are consistent with our discussions in Section 3 and our solution evaluation results in Section 4.

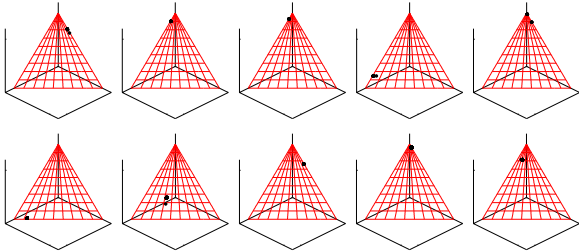


**Figure 19:** Obtained solution sets for the DTLZ1 with  $r = 1.0$  (top: population size 15, bottom: population size 100).

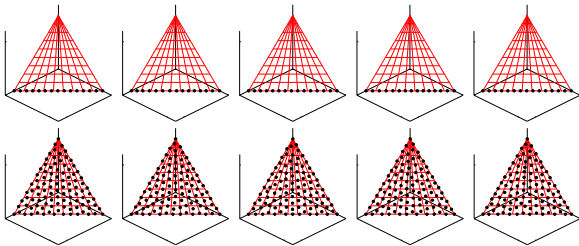


**Figure 20:** Obtained solution sets for the DTLZ1 with  $r = 1.1$  (top: population size 15, bottom: population size 100).

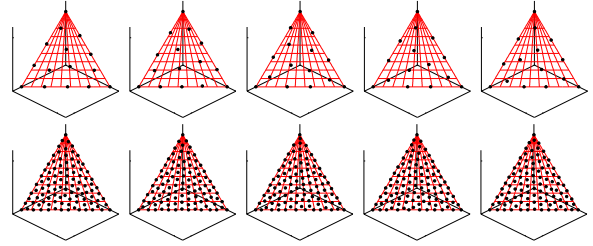


**Figure 21:** Obtained solution sets for the DTLZ1 with  $r = 1.5$  (top: population size 15, bottom: population size 100).

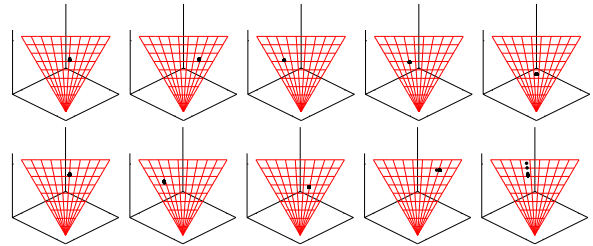


**Figure 22:** Obtained solution sets for the inverted DTLZ1 with  $r = 1.0$  (top: population size 15, bottom: population size 100).

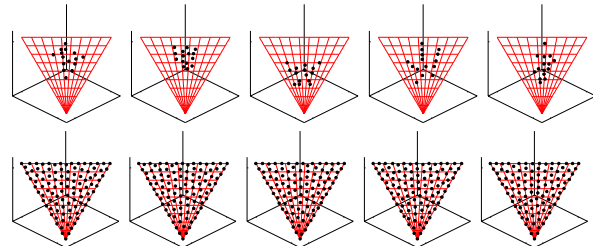


**Figure 23:** Obtained solution sets for the inverted DTLZ1 with  $r = 1.1$  (top: population size 15, bottom: population size 100).

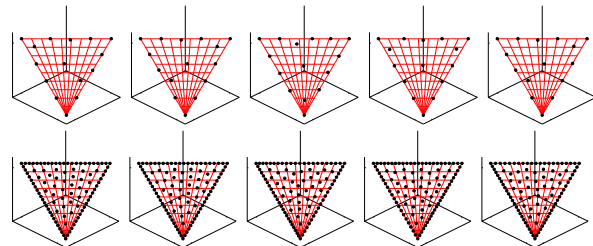


**Figure 24:** Obtained solution sets for the inverted DTLZ1 with  $r = 1.5$  (top: population size 15, bottom: population size 100).

Due to the page limitation, we cannot show all experimental results on the five-objective DTLZ1 and inverted DTLZ1 problems. In Fig. 25, we only show our experimental results on the inverted DTLZ1 problem for the case of the population size 100. Our suggested reference point is  $r = 1.25$  in this case ( $m = 5, n_{pop} = 100, H = 4$ ). In Fig. 25, good solution sets are obtained when  $r = 1.5$ . When  $r = 1.0$  in Fig. 25 (the top five results), the diversity of the obtained solutions is very small as in Fig. 19 and Fig. 22. When  $r = 1.1$  (the middle five results), the diversity of the obtained solutions is larger than the case of  $r = 1.0$ . However, the

obtained solutions are not fully covered the entire Pareto front. Especially, the best objective value of each objective (i.e.,  $f_i = 0.0$ ) is not obtained for any objective in the middle five results. When  $r = 1.5$  in Fig. 25 (the bottom five results), a wide variety of solutions are obtained over the entire Pareto front. It should be noted that the original objective values before the normalization are shown in Fig. 25 (i.e., the ideal point and the nadir point are  $(0.0, 0.0, \dots, 0.0)$  and  $(0.5, 0.5, \dots, 0.5)$  in Fig. 25).

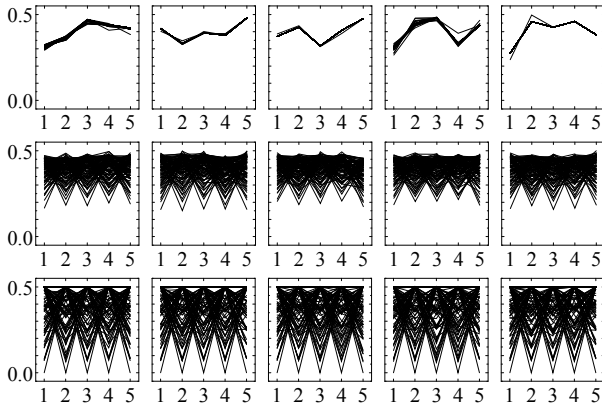


**Figure 25:** Results on the inverted DTLZ1 with the population size 100 (top:  $r = 1.0$ , middle:  $r = 1.1$ , bottom:  $r = 1.5$ ).

## 6 CONCLUSIONS

In this paper, we discussed the reference point specification in hypervolume calculation for fair performance comparison. Based on the existing theoretical studies on the optimal distribution of solutions on a linear Pareto front of a two-objective problem, we suggested the reference point specification as  $r = 1 + 1/H$  where  $H$  is the user-defined parameter for specifying the number of weight vectors in MOEA/D. Through computational experiments, we demonstrated that the suggested specification is appropriate for three-objective and five-objective test problems. We also showed that the effect of the reference point is totally different between the triangular and inverted triangular Pareto fronts. It is clearly shown that the reference point should be carefully specified for multiobjective problems with inverted triangular Pareto fronts.

## REFERENCES

- [1] A. Auger, J. Bader, D. Brockhoff, and E. Zitzler. 2012. Hypervolume-based multiobjective optimization: Theoretical foundations and practical implications. *Theoretical Computer Science* 425 (2012), 75-103.
- [2] J. Bader and E. Zitzler. 2011. HypE: An algorithm for fast hypervolume-based many-objective optimization. *Evolutionary Computation* 19, 1 (2011), 45-76.
- [3] M. Basseur, B. Derbel, A. Goëffon, and A. Liefooghe. 2016. Experiments on greedy and local search heuristics for  $d$ -dimensional hypervolume subset selection. In *Proceedings of 2016 Genetic and Evolutionary Computation Conference (GECCO 2016)*, ACM, Denver, USA, 541-548.
- [4] N. Beume, B. Naujoks, and M. Emmerich. 2007. SMS-EMOA: Multiobjective selection based on dominated hypervolume. *European Journal of Operational Research* 180, 3 (2007), 1653-1669.
- [5] K. Bringmann, T. Friedrich, and P. Klitzke. 2014. Two-dimensional subset selection for hypervolume and epsilon-indicator. In *Proceedings of 2014 Genetic and Evolutionary Computation Conference (GECCO 2014)*, ACM, Vancouver, Canada, 589-596.
- [6] D. Brockhoff. 2010. Optimal  $\mu$ -distributions for the hypervolume indicator for problems with linear bi-objective fronts: Exact and exhaustive results. In

- Proceedings of the 8th International Conference on Simulated Evolution and Learning (SEAL 2010)*, Springer, Kanpur, India, 24-34.
- [7] K. Deb, L. Thiele, M. Laumanns, and E. Zitzler. 2002. Scalable multi-objective optimization test problems. In *Proceedings of 2002 Congress on Evolutionary Computation (CEC 2002)*, IEEE, Honolulu, USA, 825-830.
- [8] T. Friedrich, F. Neumann, and C. Thyssen. 2015. Multiplicative approximations, optimal hypervolume distributions, and the choice of the reference point. *Evolutionary Computation* 23, 1 (2015), 131-159.
- [9] A. P. Guerreiro, C. M. Fonseca, and L. Paquete. 2015. Greedy hypervolume subset selection in the three-objective case. In *Proceedings of 2015 Genetic and Evolutionary Computation Conference (GECCO 2015)*, Madrid, Spain, 671-678.
- [10] A. P. Guerreiro, C. M. Fonseca, and L. Paquete. 2016. Greedy hypervolume subset selection in low dimensions. *Evolutionary Computation* 24, 3 (2016), 521-544.
- [11] S. Huband, P. Hingston, L. Barone, and L. While. 2006. A review of multiobjective test problems and a scalable test problem toolkit. *IEEE Trans. on Evolutionary Computation* 10, 5 (2006), 477-506.
- [12] H. Ishibuchi, N. Akedo, and Y. Nojima. 2015. Behavior of multi-objective evolutionary algorithms on many-objective knapsack problems. *IEEE Trans. on Evolutionary Computation* 19, 2 (2015), 264-283.
- [13] H. Ishibuchi, R. Imada, Y. Setoguchi, and Y. Nojima. 2017. Hypervolume subset selection for triangular and inverted triangular Pareto fronts of three-objective problems. In *Proceeding of the 14th ACM/SIGEVO Conference on Foundations of Genetic Algorithms (FOGA 2017)*, ACM, Copenhagen, Denmark, 95-110.
- [14] H. Ishibuchi, H. Masuda, and Y. Nojima. 2014. Selecting a small number of non-dominated solutions to be presented to the decision maker. In *Proceedings of 2014 IEEE International Conference on Systems, Man, and Cybernetics (SMC 2014)*, IEEE, San Diego, USA, 3850-3855.
- [15] H. Ishibuchi, Y. Setoguchi, H. Masuda, and Y. Nojima. 2017. Performance of decomposition-based many-objective algorithms strongly depends on Pareto front shapes. *IEEE Trans. on Evolutionary Computation* 21, 2 (2017), 169-190.
- [16] H. Jain and K. Deb. 2014. An evolutionary many-objective optimization algorithm using reference-point based non-dominated sorting approach, Part II: Handling constraints and extending to an adaptive approach. *IEEE Trans. on Evolutionary Computation* 18, 4 (2014), 602-622.
- [17] T. Kuhn, C. M. Fonseca, L. Paquete, S. Ruzika, M. M. Duarte, and J. R. Figueira. 2016. Hypervolume subset selection in two dimensions: Formulations and algorithms. *Evolutionary Computation* 24, 3 (2016), 411-425.
- [18] K. Li, K. Deb, Q. Zhang, and S. Kwong. 2015. An evolutionary many-objective optimization algorithm based on dominance and decomposition. *IEEE Trans. on Evolutionary Computation* 19, 5 (2015), 694-716.
- [19] H. Seada and K. Deb. 2016. A unified evolutionary optimization procedure for single, multiple, and many objectives. *IEEE Trans. on Evolutionary Computation* 20, 3 (2016), 358-369.
- [20] P. K. Shukla, N. Doll, and H. Schmeck. 2014. A theoretical analysis of volume based Pareto front approximations. In *Proceedings of 2014 Genetic and Evolutionary Computation Conference (GECCO 2014)*, ACM, Vancouver, Canada, 1415-1422.
- [21] T. Wagner, N. Beume, and B. Naujoks. 2007. Pareto-, aggregation-, and indicator-based methods in many-objective optimization. In *Proceedings of the 4th International Conference on Evolutionary Multi-Criterion Optimization (EMO 2007)*, Springer, Matsushima, Japan, 742-756.
- [22] Y. Yuan, H. Xu, B. Wang, and X. Yao. 2016. A new dominance relation based evolutionary algorithm for many-objective optimization. *IEEE Trans. on Evolutionary Computation* 20, 1 (2016), 16-37.
- [23] Y. Yuan, H. Xu, B. Wang, B. Zhang, and X. Yao. 2016. Balancing convergence and diversity in decomposition-based many-objective optimizers. *IEEE Trans. on Evolutionary Computation* 20, 2 (2016), 180-198.
- [24] Q. Zhang and H. Li. 2007. MOEA/D: A multiobjective evolutionary algorithm based on decomposition. *IEEE Trans. on Evolutionary Computation* 11, 6 (2007), 712-731.
- [25] E. Zitzler, D. Brockhoff, and L. Thiele. 2007. The hypervolume indicator revisited: On the design of Pareto-compliant indicators via weighted integration. In *Proceedings of the 4th International Conference on Evolutionary Multi-Criterion Optimization (EMO 2007)*, Springer, Matsushima, Japan, 862-876.
- [26] E. Zitzler and L. Thiele. 1998. Multiobjective optimization using evolutionary algorithms - A comparative case study. In *Proceedings of the 5th International Conference on Parallel Problem Solving from Nature (PPSN V)*, Amsterdam, Netherlands, 292-301.
- [27] E. Zitzler, L. Thiele, M. Laumanns, C. M. Fonseca, and V. G. da Fonseca. 2003. Performance assessment of multiobjective optimizers: An analysis and review. *IEEE Trans. on Evolutionary Computation* 7, 2 (2003), 117-132.